Proangiogenic contribution of adiponectin toward mammary tumor growth in vivo

Published in final edited form as:
Clin Cancer Res. 2009 May 15; 15(10): 3265–3276. doi:10.1158/1078-0432.CCR-08-2649.

Proangiogenic Contribution of Adiponectin toward Mammary Tumor Growth *In vivo*

Shira Landskroner-Eiger[1], **Binzhi Qian**[2], **Eric S. Muise**[4], **Andrea R. Nawrocki**[1], **Joel P. Berger**[5], **Eugene J. Fine**[3], **Wade Koba**[3], **Yingfeng Deng**[6], **Jeffrey W. Pollard**[2], and **Philipp E. Scherer**[6]

[1]Department of Cell Biology, Center of Reproductive Biology and Womens' Health, Albert Einstein Cancer Center, Bronx, New York

[2]Department of Developmental and Molecular Biology, Center of Reproductive Biology and Womens' Health, Albert Einstein Cancer Center, Bronx, New York

[3]Department of Nuclear Medicine, M. Donald Blaufox Laboratory for Molecular Imaging, Albert Einstein College of Medicine, Bronx, New York

[4]Department of Molecular Profiling, Merck Research Laboratories, Rahway, New Jersey

[5]Department of Metabolic Disorders, Merck Research Laboratories, Rahway, New Jersey

[6]Touchstone Diabetes Center, Departments of Internal Medicine, Cell Biology and Simmons Cancer, University of Texas Southwestern Medical Center, Dallas, Texas

Abstract

Purpose—Adipocytes represent one of the most abundant constituents of the mammary gland. They are essential for mammary tumor growth and survival. Metabolically, one of the more important fat-derived factors ("adipokines") is adiponectin (APN). Serum concentrations of APN negatively correlate with body mass index and insulin resistance. To explore the association of APN with breast cancer and tumor angiogenesis, we took an *in vivo* approach aiming to study its role in the mouse mammary tumor virus (MMTV)-polyoma middle T antigen (PyMT) mammary tumor model.

Experimental Design—We compared the rates of tumor growth in MMTV-PyMT mice in wild-type and APN-null backgrounds.

Results—Histology and micro-positron emission tomography imaging show that the rate of tumor growth is significantly reduced in the absence of APN at early stages. PyMT/APN knockout mice exhibit a reduction in their angiogenic profile resulting in nutrient deprivation of the tumors and tumor-associated cell death. Surprisingly, in more advanced malignant stages of the disease, tumor growth develops more aggressively in mice lacking APN, giving rise to a larger tumor burden, an increase in the mobilization of circulating endothelial progenitor cells, and a gene expression fingerprint indicative of more aggressive tumor cells.

Requests for reprints: Philipp E. Scherer, Touchstone Diabetes Center, The University of Texas Southwestern Medical Center, 5323 Harry Hines Boulevard, Dallas, TX 75390-8549. Phone: 214-648-8715; Fax: 214-648-8720; philipp.scherer@utsouthwestern.edu. Current address for A.R. Nawrocki: Department of Metabolic Disorders, Merck Research Laboratories, Rahway, NJ 07065.

Note: Supplementary data for this article are available at Clinical Cancer Research Online (http://clincancerres.aacrjournals.org/).

Disclosure of Potential Conflicts of Interest
No potential conflicts of interest were disclosed.

Conclusions—These observations highlight a novel important contribution of APN in mammary tumor development and angiogenesis, indicating that APN has potent angio-mimetic properties in tumor vascularization. However, in tumors deprived of APN, this antiangiogenic stress results in an adaptive response that fuels tumor growth through mobilization of circulating endothelial progenitor cells and the development of mechanisms enabling massive cell proliferation despite a chronically hypoxic micro-environment.

The physiologic role of adipose tissue as a dynamic organ has shown its crucial role in maintaining normal systemic energy balance, glucose homeostasis, and the immune response (1, 2). In the context of the mammary gland, the adipocytes are an abundant cell type in the stroma and are vital for ductal development and survival. This is due largely to their secretory profile of adipokines such as leptin, adiponectin, hepatocyte growth factor, collagen VI, interleukin 6, and tumor necrosis factor α (3). Mammary tumor growth is determined by cell-autonomous effects of epithelial cancer cells as well as by contributions of the stromal compartment (4–6). Here, we focus on the adipocyte microenvironment of the mammary gland. Our previous work characterized a broad spectrum of effects mediated by soluble adipokines on the proliferative, invasive, and angiogenic capacity of ductal epithelial cells (5, 7), suggestive of major contributions of adipokines to the malignant progression of breast cancer.

A widely studied adipokine in the area of metabolism is adiponectin (APN; ref. 8). APN is an adipocyte-specific secretory protein that enhances hepatic insulin sensitivity by suppressing hepatic glucose output from gluconeogenesis (9, 10) and also affects glucose uptake in the muscle (11). In addition, it has potent protective effects against inflammation, adverse lipid profiles, and atherosclerosis. As a result, it is thought to be potently cardioprotective (11, 12).

Recently, a great deal of attention has been given to the study of the epidemiologic association between APN levels in circulation and breast cancer incidence. It is generally accepted that obesity is a risk factor for breast cancer in postmenopausal but not premenopausal women (13). Because APN levels are inversely correlated with obesity (11), it has been suggested that the decreased levels of APN may explain the increased risk of breast cancer in obesity (13, 14). The epidemiologic association between APN levels and breast cancer incidence suggested an inverse correlation between APN and breast cancer risk, an association that seems to be stronger for postmenopausal women (14, 15). *In vitro* assays have studied the APN-mammary cancer axis, suggesting an inhibitory role for APN in mammary tumor growth (16, 17). Similar results were obtained after intratumoral injection of APN into fibrosarcoma tumors (18). In the majority of these cases, bacterially produced forms of APN were used either *in vitro* or in the xenograft models, conditions with limited relevance for the physiologic action of endogenous, full-length APN, and autochthonous tumors. Due to its highly complex tertiary and quaternary structure, APN has to be synthesized in a mammalian production system to recapitulate the complex nature of its endogenous counterpart (9). In addition, xenograft models may not accurately predict the antiangiogenic and antitumor responses in human tumors (19, 20).

Thus, we took a direct *in vivo* approach, using our previously generated APN knockout (KO) mice (21), to decipher the role of APN and its effect on mammary tumor growth with the widely used mouse mammary tumor virus (MMTV)-polyoma middle T antigen (PyMT) model, a spontaneous mammary tumor model (22). This tumor model has been shown to recapitulate many processes found in human breast cancer progression both morphologically and in the pattern of expression of biomarkers associated with poor prognosis (23). The APN KO mice develop diet- and obesity-induced insulin resistance (21, 24) and an impaired angiogenic response to ischemia (25), but have, in an unchallenged state, minimal

phenotypic manifestations. We observed that in early stages of tumor progression, lack of APN delays tumor growth by inhibiting angiogenesis in a paracrine and/or endocrine fashion.

Despite the defects in angiogenesis in early stages of tumorigenesis in APN KO mice, tumor growth persisted, leading to rapid tumor growth at later stages of carcinoma. This involved increased levels of vascular endothelial growth factor (VEGF)-A in the tumor, the mobilization of circulating endothelial progenitor cells (CEP), and the emergence of a vasculature with normal appearance as opposed to the dilated and distorted shape characteristic of tumor vessels. We hypothesized that in mice lacking APN, the antiangiogenic stress at early stages leads to an adaptation mechanism during which CEPs are mobilized to contribute to tumor growth, similar to other tumor models undergoing antiangiogenic stress (26–28).

Combined, our observations indicate that APN has potent angio-mimetic properties in the early steps of tumor vascularization where mice lacking APN have a lagging angiogenic response. However, this antiangiogenic stress triggers an adaptive reaction that fuels tumor growth at later stages. The present data suggest a possible mechanism for the increased risk and poorer prognosis seen in breast cancer patients with low serum APN levels (such as obese women) due to acquired adaptation of tumors to antiangiogenic stress.

Materials and Methods

Animals

All animal experimental protocols were approved by the Institute for Animal Studies of the Albert Einstein College of Medicine and by the Institutional Animal Care and Use Committee of University of Texas Southwestern Medical Center at Dallas. Mice were maintained as described previously (29). Experiments presented were done on a mixed C57/Bl6 and FVB background or a pure FVB background (an excess of nine backcrosses; Figs. 1D, 2, 3, 5, and 6; Supplementary Figs. S1C–D and S2). The majority of experiments were done on both genetic backgrounds with similar results. Double heterozygous PyMT/ APN males were crossed with APN heterozygous females to obtain littermates that are deficient for APN or wild type (WT). Further experimental cohorts were generated by crossing the heterozygous PyMT/APN KO males to APN KO females, and male heterozygous PyMT to WT females (21). Intermittently, animals were bred as male PyMT/APN heterozygous at both loci crossed to APN heterozygous females. Mammary tumor development was compared between age-matched females of PyMT and PyMT/APN null mice. For detection of mammary tumor volume, mice were monitored biweekly. Tumor diameter was measured with a caliper, and tumor volume calculated as $(H \times W^2)/2$. APN-over-expressing mice were previously obtained and characterized (29).

Whole-mount staining and histology of mammary gland

For histology, inguinal mammary glands were fixed for 24 h in 10% normal buffered formalin (Fisher) and embedded in paraffin. Five-micrometer sections were stained with H&E; two to three sections per mouse were examined for tumor staging in a blind fashion and staged as described previously (23). Whole-mount staining was done as described,[7] imaged on a Stemi SV11 stereo dissection microscope, and analyzed for lesion area using Image J software.

[7]http://mammary.nih.gov/

Morphologic analysis of mammary gland development

To determine ductal lengths, mammary gland whole-mount preparations were analyzed by measuring the distance of the three longest ducts from the edge of the 4th mammary gland at the interface with the 5th mammary gland to the leading edge of the mammary gland. Terminal end buds were counted in the whole mammary gland.

Peroxisome proliferator–activated receptor-γ agonist regimen

The peroxisome proliferator–activated receptor-γ (PPARγ) agonist 2-(2-(4-phenoxy-2-propylphenoxy)ethyl)indole-5-acetic acid (COOH) was a kind gift from Merck Research Laboratories. The drug was mixed with a standard chow diet powder at 10 mg/kg body weight/d and mice were treated from 4 until 9 wk of age. The mice were subjected to tail bleeding before and during the course of the treatment.

Immunohistochemistry analysis—CD31 and terminal deoxyribonucleotidyl transferase–mediated dUTP nick end labeling

Inguinal mammary glands were evaluated for the presence of microvessels on sections fixed 24 h in Zinc Fixative (BD Pharmingen) and stained with antimouse platelet endothelial cell adhesion molecule/CD31 antibody (BD Pharmingen) overnight at 4°C (1:30). Biotinylated secondary antibodies were detected with a DAB Substrate Chromagen System (DakoCytomation). The CD31-positive blood vessels in PyMT and PyMT/APN KO derived specimens were counted in four fields having the maximal number of CD31-positive staining per unit area of a section [modification of Weidner et al. (30)]. These were averaged to calculate the micro-vessel density. Vessel imaging on frozen sections was carried out with a 1:50 dilution of antimouse platelet endothelial cell adhesion molecule/CD31 antibody (BD Pharmingen) and a secondary antibody labeled with Alexa Fluor 488 at 1:200 (Molecular Probes). Nuclei were detected with 4′,6-diamidino-2-phenylindole. Terminal deoxyribonucleotidyl transferase–mediated dUTP nick end labeling (TUNEL) staining was done according to the manufacturer's protocol (Chemicon), and 10 random fields from areas of lesions were imaged per mouse for further analysis. Sections were imaged using the Zeiss Axioskop Plus with the AxioCam MRc camera or Olympus IX81 microscope.

In vivo vessel labeling

Texas red–conjugated dextran (MW 70,000; Molecular Probes) was prepared at 6.2 mg/mL in PBS. One hundred microliters were injected i.v., and 5 min after the injection, mice were sacrificed and inguinal mammary glands were fixed in 10% buffered formalin to be processed by standard procedures (6). For analysis, samples were further stained with 4′,6-diamidino-2-phenylindole and imaged using the Olympus IX81 microscope. Every second field of tissue section was imaged, of which 10 random images per mouse were further quantified using Image J software.

APN, leptin, insulin, and glucose measurements

APN was measured from tail blood with a mouse adiponectin RIA kit (LINCO Research) or by Western blot analysis with rabbit polyclonal anti-mouse APN antibody. The bands were detected by the Odyssey Infrared Imaging System (LI-COR) and band intensity was quantified with Odyssey v1.2 software (LI-COR Biotechnology). Leptin levels were measured using the mouse leptin Elisa kit (LINCO Research). Insulin, glucose, and oral glucose tolerance tests were done as described (29).

APN neutralization and APN injections

For APN neutralization experiments, 5-wk-old PyMT females were injected i.p. for a 2-wk period with either antimouse APN monoclonal antibodies (clones 14 and 45) or purified

mouse IgGs (Sigma) at 50 μg per mouse every 3rd day (31). APN protein levels were monitored from tail blood by Western blot analysis.

For APN injections, APN KO and WT male littermates were injected with a preparation of APN enriched in high molecular weight form (~70% of high molecular weight). Mice were anesthetized briefly with isoflurane, and APN was delivered through retro-orbital injections at a concentration of 1 μg/g body weight. Injections were done at 10 a.m. and 6 p.m. on day 1 and at 10 a.m. on day 2. After the last injection, food was removed and animals were fasted for 4 h before isolation of tissues. Epididymal fat was collected and flash-frozen in liquid nitrogen.

In vivo Matrigel plug assays

Female mice (10–12 wk of age) were briefly anesthetized and injected s.c. at the abdominal upper midline with 0.5 mL of Matrigel (BD Biosciences) either supplemented with 100 ng/mL of basic fibroblast growth factor (FGF; PeproTech, Inc.) or without basic FGF as a negative control. Mice were sacrificed 10 d after injection and Matrigel plugs were excised and fixed in Zinc Fixative for 24 h at room temperature. For histologic analysis, paraffin-embedded sections were stained for H&E. A total of nine sections per Matrigel were imaged in regions of highest population. Cell density per Matrigel area was quantified using Image J software.

[^{18}F]Fluorodeoxyglucose positron emission tomography imaging

PyMT and PyMT/APN KO mice were fasted 2 to 3 h before a tail vein injection of [^{18}F]fluorodeoxyglucose ([^{18}F]FDG; 300 μCi). One hour after injection, mice were subjected to positron emission tomography (PET) scanning with the Concorde Microsystems R4 microPET Scanner. Animals were imaged while anesthetized through inhalation with isoflurane. Image acquisition was done using the MicroPET Manager with the ASPIRO dedicated software. For analysis, manual regions of interest were defined around areas of visually identified mammary gland activity. Successive two-dimensional slices (each 1.2 mm thick in the axial images), after stacking, derived a volume fitted to each mammary gland. The counts per cubic centimeter within this volume multiplied by the fitted volume provided total percent of injected dose against the calibrated injection activity. The glucose uptake was measured for all 10 mammary glands by calculating the percentage of uptake in the mammary gland relative to the injected dose of the [^{18}F]FDG normalized to body weight.

RNA isolation and analysis

Mice were sacrificed, and tissue was immediately harvested and frozen in liquid nitrogen. RNA was isolated from frozen mammary gland tissue by using the Qiagen RNeasy Lipid tissue kit following the manufacturer's protocol. cDNA was synthesized from 5 μg RNA using Superscript III and oligo dT (Invitrogen). All PCR reactions were normalized to actin mRNA. Quantitative PCR, using SYBR Green I master mix, was done in the Roche Lightcycler 480. Primer sequences are listed in Supplementary Fig. S4.

Flow cytometry

Blood was obtained from anesthetized mice through cardiac puncture and was followed by red blood lysis. Cells were stained with FITC-, allophycocyanin-, phycoerythrin-, or biotin-conjugated antibodies against murine CD45 (e-Biosciences), CD31 (BioLegend), VEGF receptor (VEGFR)-1 (R&D), and VEGFR-2 (R&D). CEPs were identified by double positivity for VEGFR-2 and CD31 and double negativity for VEGFR-1 and CD45. Viable

cells were distinguished from dead cells by using 4′,6-diamidino-2-phenylindole staining. Cells were measured by LSR II flow cytometer and analyzed using FlowJo software.

Body composition analysis

Body composition was measured using an Echo magnetic resonance imaging system (Echo Medical Systems).

Gene expression profiling for animals injected with APN

Male animals were euthanized by CO_2 asphyxiation 4 h after the final treatment dose, and epididymal white adipose tissue was harvested and flash-frozen in liquid nitrogen. Total RNA was isolated after homogenizing the frozen tissues in Trizol reagent (Invitrogen) and processed using RNeasy kits (Qiagen) according to the manufacturers' instructions. Microarray processing was done as previously described (32). Briefly, labeled cRNA was hybridized for 48 h onto Agilent 60-mer two-color spotted micro-arrays. Individual strain or compound treatment samples (including individual control or vehicle treatment samples) were hybridized against a control or vehicle treatment pool. Fold change and *P* values were generated by averaging replicates (two to three replicates per strain or treatment) and using the Rosetta Resolver v6.0 software (Rosetta Inpharmatics LLC, a wholly owned subsidiary of Merck & Co., Inc.). Fold change values represent the difference in regulation of the treatment samples versus the control samples, with a positive value signifying up-regulation following treatment and vice versa.

Gene expression profiling for late-stage tumors

cDNA synthesis was done on pooled RNA from two to three animals per group. Three independent groups per genotype were hybridized to an Illumina mouse whole-genome expression beadchip MouseWG-6. Microarray data were analyzed using Partek Genomic Suite Software and Ingenuity Pathways Analysis. For the Ingenuity Pathways Analysis, genes were filtered using the criteria $P < 0.03$.

Statistical analysis

Results are shown as mean ± SE of all experiments combined. Experiments were done thrice independently (except the Matrigel *in vivo* assays and PET imaging, which were repeated twice independently). Statistical analysis was done by Student's *t* test or two-way ANOVA analysis and subsequent Tukey test using Prism 4.0 or SigmaStat version 2.03. Significance was accepted at $P \leq 0.05$.

Results

Mammary tumorigenesis in PyMT/APN KO mice is delayed

We sought to test whether MMTV-PyMT–driven mammary tumor growth is affected by the absence of APN. Having shown that lack of APN is dispensable for mammary development (Supplementary Fig. S1A and B), in contrast to the altered ductal architecture in mice overexpressing APN (Supplementary Fig. S1C and D), we decided to focus on the phenotypic analysis of the loss of function of APN rather than the gain-of-function model. Whole-mount preparations were analyzed for mammary tumor growth at 5 and 7 weeks of age. Lesion areas in PyMT and PyMT/APN KO mice were comparable at 5 weeks of age, yet mice lacking APN showed a 50% reduction in lesion area compared with PyMT by 7 weeks of age (14.1 ± 2.3 versus 7 ± 0.7 mm^2; Fig. 1A, *top* and *bottom*). Similarly, a histologic analysis of mammary glands examined at 7 weeks of age revealed that 38% of the PyMT have transitioned into the malignant stage (i.e., early carcinoma or late carcinoma stage), in contrast to only 15% of the PyMT/APN KO mice (Fig. 1B). In addition, PyMT/

APN KO had a delayed onset of palpable tumors compared with PyMT mice (data not shown). This time course analysis of the inguinal glands suggests that mammary tumorigenesis may critically depend on APN during the early stages of tumor progression.

APN neutralization mimics PyMT/APN KO phenotype

Whereas the genetic model with a disruption of the *APN* gene has great advantages, we cannot formally rule out the possibility that the absence of APN during development causes secondary effects that escaped our analysis. To address this issue in a more acute setting, we took advantage of two monoclonal antibodies that we have generated against mammalian-produced recombinant mouse APN (31). This injection protocol effectively triggers the clearance of circulating APN, thereby lowering its concentrations in serum sharply by 75% to 80%. As a control, mice were injected with nonimmune mouse IgGs, a process that did not alter APN levels in circulation (Fig. 1C, *top*). Because the APN-null model suggested a critical involvement of APN around 7 weeks of age in PyMT mice, we started the antibody treatment at week 5 and maintained the systemic lowering of APN for 2 weeks with repeated injections of antibodies every 3 days. Consistent with the chronic depletion of APN, lowering of APN levels with an antibody-mediated approach showed similar trends with a 2-fold reduction in lesion area, suggesting that APN plays an important role in maintaining mammary tumor progression at this stage (Fig. 1C, *bottom*).

PPARγ agonists accelerate tumorigenesis—a gain-of-function analysis

PPARγ, a member of the nuclear hormone receptor superfamily, is an integral regulator of energy homeostasis and has a central role in the differentiation of adipocytes (33). It has also been shown to regulate cell growth and differentiation of a variety of cancer cells, yet its involvement in the different cancer models is controversial (34). Clinically, APN circulating levels are highly up-regulated in response to treatment with PPARγ agonists, such as the thiazolindinediones (35). This up-regulation of APN is an integral component of the antidiabetic activity of these compounds. In light of the pluripotent effects of PPARγ agonists that include up-regulation of APN, this is an effective tool to test for the effects of elevated systemic APN levels on mammary gland tumor development. Starting at 4 weeks of age, PyMT mice were fed a standard chow diet or a standard chow diet supplemented with the PPARγ agonist COOH for a duration of 5 weeks. Measurements of circulating APN showed a 3-fold increase in APN serum levels by day 6 of treatment (data not shown). An integrated assessment of whole-mount analysis shows a 35% increase in lesion area in PyMT mice treated with the PPARγ agonist COOH compared with control PyMT. This is in contrast to a more modest increase of 21% in lesion area in PyMT/APN KO mice treated with PPARγ agonist compared with control PyMT/APN KO (Fig. 1D). These observations are consistent with the notion that PPARγ activators may promote mammary tumor growth at early stages partially through induction of APN. This may be generally relevant for all tumor types invading stromal compartments enriched in adipocytes.

Loss of APN predisposes to reduced tumor glucose uptake and increased tumor-associated death

PET imaging is a valuable method that is widely used clinically and in animal models of cancers, allowing to monitor the presence and progression of tumors using a positron emitting tracer. To further monitor the mammary tumor progression, PET imaging was applied using [^{18}F]FDG as a measurement of tumor glucose uptake (36). At 9 weeks of age, in accordance with the dramatic increase of metabolism that occurs during tumor development (36), [^{18}F]FDG uptake was elevated in the mammary glands of PyMT mice. In contrast, only modest levels of [^{18}F]FDG were accumulated in the mammary glands of age-matched PyMT/ APN KO animals. The glucose uptake was measured for all 10 mammary

glands, showing an 11-fold increase in the [^{18}F]FDG uptake in PyMT mammary glands compared with age-matched PyMT/APN KO mammary glands (Fig. 2A).

A histologic examination at this age group revealed necrotic regions in 20% of PyMT/APN KO mice. In contrast, none of the age-matched PyMT presented such characteristics (Fig. 2B). TUNEL staining revealed a 43% increase in TUNEL-positive cells in mammary lesions of PyMT/APN KO compared with PyMT mice (Fig. 2C). This suggests that lack of APN at this time frame of tumor progression limits the availability of glucose and other nutrients for the tumor environment, leading to a nutrient-deprived cell mass susceptible to cell death and limiting tumor progression.

APN as a positive regulator of angiogenesis

Previous work has proposed a role for APN in vessel remodeling and promotion of angiogenesis in an *in vivo* hind limb model of ischemia (25, 37). To obtain a comprehensive overview of the angiogenic potential of APN, independent of tumor cells, WT mice were exposed to a series of APN injections for 2 days, followed by microarray gene expression profiling of white adipose tissue. The mRNA expression profile points to an induction of key proangiogenic markers, the most robust effect being on VEGF-A (1.6-fold), VEGF-B (1.5-fold), VEGFR2 (1.65-fold), and VEGFR1 (1.4-fold; Fig. 3A).

To functionally validate whether APN can mediate its proangiogenic effect independent of the tumor cells, basic FGF–impregnated Matrigel Matrix preparation was s.c. injected into either WT or APN KO mice to assess recruitment of vascular endothelial cells. A histologic examination showed that Matrigel explants from APN KO mice had a significantly lower cellular content (2.2-fold) with fewer infiltrating cells compared with those from WT control mice (Fig. 3B). As a negative control, Matrigel devoid of basic FGF was injected, resulting in very few infiltrating cells in both groups (data not shown). The presence of vascular channels was examined by immunostaining with anti-CD31 antibody. Figure 3C reveals elevated blood vessel content in WT compared with the APN KO derived Matrigel. Combined, these observations lend support for a systemic angiogenic and promigratory environment in the presence of APN by promoting recruitment of endothelial cells and possibly additional stromal subpopulations, in addition to shaping the angiogenic profile by controlling the expression of key factors that are of great potential as targets for antiangiogenic therapy.

Tumor vasculature in PyMT/APN KO mice is impaired

Given the proangiogenic role of APN in the *in vivo* model, we reasoned that the lack of APN may prominently lead to deficiencies under conditions when vascularization is rate-limiting. We sought to examine the contribution of APN on tumor-associated angiogenesis at times when lesions have progressed from a pre-malignant to a malignant stage. Total VEGF-A mRNA levels measured in the mammary gland showed a 2.3-fold increase in PyMT compared with PyMT/APN KO mice (Fig. 4A). Similarly, mRNA levels of additional angiogenic markers such as CD31 (1.8-fold), von Willebrand factor (2.3-fold), and VEGFR1 (2.1-fold) were detected at increased levels in PyMT compared with PyMT/APN KO mice (Fig. 4A). Consistent with these results, immunostaining with anti-CD31 antibody revealed a 2-fold increase in microvessel density in the mammary glands of PyMT mice relative to PyMT/APN KO mice (Fig. 4B).

The density of functional vascularization was further assessed by *in vivo* labeling of the blood vessels using an i.v. injection of Texas red–conjugated dextran (6). We show that in the absence of APN, tumors are likely to have diminished functional vascular density (Fig.

4C and D). This strongly suggests that APN promotes tumor growth, at least in part, by promoting an angiogenic response during lesion expansion.

Changes in APN levels during tumor expansion

We examined the fluctuations in circulating plasma APN levels over the course of tumor progression in the PyMT model. By 12 weeks of age, a time point when tumors characteristically advance to late carcinoma, circulating APN levels were reduced by 44% in tumor-bearing PyMT mice compared with their WT littermates [Supplementary Fig. S2A(*a*)]. Other circulating adipokines such as leptin were down-regulated in both models independently of the presence of tumors [Supplementary Fig. S2A(*b*)]. These results show that APN levels at late tumor stages may not be indicative of the pivotal role of APN at the early stage of tumorigenesis when its circulating levels are more prevalent, and highlight the complex dynamic relationship of the tumor with its microenvironment.

In spite of the dramatic reduction in APN levels, fasting glucose and insulin levels were unaltered as was the glucose excursion during an oral glucose tolerance test done at both early and late stages of tumor progression (Supplementary Fig. S3). The decline in APN occurs despite the reduction in fat mass as assessed by whole-body Echo magnetic resonance imaging analysis (Supplementary Fig. S2B). Loss in fat mass is generally associated with an increase in plasma APN levels and a positive effect on insulin sensitivity. In our tumor model, the loss of fat mass does not trigger an increase in APN. This may be caused by increased local inflammation in the mammary fat pads or may simply be a reflection of adipocyte loss in the context of increased tumor burden in the mammary fat pad.

Bypass of the antiangiogenic stress in late-stage mammary tumors of APN KO mice

We next probed for the effects of APN at later stages of tumor progression by measuring tumor volume. Surprisingly, tumor growth in PyMT/APN KO mice not only caught up but even far exceeded tumor growth in age-matched PyMT mice at advanced stages of tumorigenesis, reaching a significant 2.2-fold difference in tumor volume by 14 weeks of age (Fig. 5A). Differences were also shown histologically: Large solid tumors with some necrosis in central local regions were present in the PyMT/APN KO tumors, whereas the PyMT-derived tumors revealed significantly smaller solid tumor regions and no necrotic regions (data not shown).

PET was applied at this late stage. In contrast to the modest levels of [^{18}F]FDG accumulation in 9-week-old PyMT/APN KO animals [Fig. 2A(*a*–*b*)], 12-week-old PyMT/APN KO mice showed a massive increase in uptake of [^{18}F]FDG into the mammary glands (Fig. 5B). This is in agreement with our advanced malignancy phenotype and correlates with the epidemiologic association of an inverse association between APN and breast cancer risk (14, 15). Our data suggest that these late-stage tumors arising from a long-term nutrient-deprived environment in the absence of APN adapt to the anaerobic conditions and emerge as very aggressive and metabolically highly active cells at later stages in spite of the presence of an initially deficient vasculature. This coincides with a provocative concept that has emerged involving the hypothesis that tumors can acclimatize to the presence of antiangiogenic stress by adaptive mechanisms that may reinitiate and induce tumor growth (26).

Induced mobilization of CEPs in acclimatized PyMT/APN KO mice

Antiangiogenic treatment can cause recruitment of various bone marrow–derived cells that have the capacity to fuel tumor growth (26, 28, 38). These bone marrow–derived cells consist of vascular progenitors and vascular modulatory cells (26). We hypothesized that

following a period of angiogenic and nutrient deprivation in mice lacking APN, the mobilization of bone marrow–derived cell subpopulations would be unique to the PyMT/APN KO mice at late-stage tumorigenesis and may contribute to the rapid surge in growth of tumors, similar to the situation in tumors that are exposed to pharmacologic antiangiogenic treatments.

We thus studied mice of both early-stage and late-stage tumors (9 and 12 weeks, respectively) and assessed circulating bone marrow–derived cell subpopulations in both PyMT and PyMT/APN KO mice using fluorescence-activated cell sorting. Differences were observed for CEPs defined as $CD45^{-}/CD31^{+}/VEGFR2^{+}/VEGFR1^{-}$ (27). Differences were observed only for late-stage tumor–bearing mice, with PyMT/ APN KO showing a 6-fold increase in circulating levels of CEP subpopulations compared with the age-matched PyMT animals (Fig. 6A).

Several secreted factors such as stromal-derived factor (SDF-1) and VEGF-A have been implicated in the recruitment of CEPs into the tumor mass through an endocrine pathway (4, 27). There is also evidence that adipose tissue capillary endothelial cells may secrete SDF-1 (39). We thus measured serum levels of SDF-1 in PyMT and PyMT/APN KO mice. In the advanced tumor stage, SDF-1 circulating levels were increased by 24% in the PyMT/APN KO compared with PyMT mice. However, this was not statistically significant (data not shown). Thus, SDF-1 may provide, at best, only a partial mechanism for CEP recruitment in our model. We further measured total VEGF-A mRNA levels in tumors, showing a 2.4-fold up-regulation in PyMT/APN KO compared with PyMT-derived tumors (Fig. 6B). This correlates with work by others showing increased VEGF-A expression in mice treated with antiangiogenic inhibitors and was even proposed as a predictive biomarker of tumor response (26).

We further examined the angiogenic milieu of these late-stage tumors. In contrast to the elevated VEGF-A mRNA levels measured at this stage (Fig. 6B), other angiogenic markers that had shown to be decreased in the PyMT/APN KO at the early stage, such as CD31 (1.3-fold), VEGFR1, and VEGFR2 (Fig. 4), were still either down-regulated or unaltered, respectively, in the PyMT/APN KO compared with PyMT tumors. This strongly suggests an alternative pathway of inducing tumor growth when the tumors are deprived of APN for an extended period of time.

We further examined the tumor vessels to evaluate whether the presence of high levels of VEGF-A in the tumor is indicative of tumor revascularization, implicating a mechanism to effectively cope with the absence of APN. No difference was observed in total blood vessel density. However, qualitatively, the majority of vessels in the PyMT tumors exhibited dilated and distorted tumor vessels, indicative of vessel remodeling. In contrast, tumor vessels derived from mice lacking APN showed vessels that were slim, elongated, and with few tortuous structures, all reflective of normal vasculature [ref. 40; Fig. 6C(*a*–*b*)]. These elongated blood vessels were seen in many cases as major vessels rather than the small, scattered blood vessels observed in the PyMT tumors [Fig. 6C(*c*–*d*)]. This is consistent with our initial observation that APN is an angio-mimetic adipokine, and it is evident that these late-stage tumors still lag behind in their angiogenic response.

Transcriptional signature of late-stage APN KO mammary tumors

Given the clinical importance of identifying key factors that are turned on at these advanced stages of the disease, we decided to use DNA microarrays to more globally asses the differences in gene expression of late-stage PyMT/APN KO and PyMT tumor samples. Cluster analysis depicted in Table 1 shows that the most robust differences were observed in the cancer cluster. A general down-regulation of tumor suppressors such as caveolin 1 (1.4-

fold) and Rb (1.3-fold) and up-regulation of antiapoptotic genes such as BFAR (4.5-fold) and DDIT4 (1.6-fold) was observed, in line with our observation of a tumor growth surge in the absence of APN at this stage of the disease. Importantly, central regulators of angiogenesis such as matrix metalloproteinase 2 (1.6-fold) and FGF1 (2.9-fold) remained clearly diminished despite the up-regulation of hypoxia-inducible factor 1α (1.5-fold) and CXCR4 (1.3-fold). A further reflection of the continued hypoxic environment in these tumors is the up-regulation of glycolytic genes such as phosphoglycerate kinase 1 and triosephosphate isomerase 1. These late-stage tumors arising under chronic hypoxic conditions in the PyMT/APN KO mice have a distinct transcriptional fingerprint that is fully consistent with a gene expression signature associated with a dramatically more aggressive tumor phenotype.

Discussion

APN has been implicated in attenuating mammary tumor progression in studies using *in vitro* or xenografts models, partially attributable to a postulated role as a negative regulator of angiogenesis (16–18). However, because there are important differences between the mechanism of tumor growth and angio-genesis in transplanted and autochthonous tumors (19, 20, 28), we have analyzed, for the first time, the role of APN in mammary tumor progression *in vivo* using the spontaneously occurring mammary tumor model of MMTV-PyMT. We did this through the use of APN KO mice and by taking advantage of neutralizing monoclonal antibodies that effectively clear APN from circulation. Contrary to the published data (16–18), we show that APN can accelerate mammary tumor growth *in vivo* at early stages when tumor lesions start to critically depend on angiogenesis for continued oxygen and nutrient supply. Such a role was also implied in an elegant recent article that was published in the course of the preparation of this article (41). These authors suggested the existence of a molecular cross talk between the putative APN receptor T-cadherin and mammary tumor growth.

Previous *in vivo* work found that APN promotes angiogenesis in response to tissue ischemia through the activation of an AMP protein kinase AMPK–dependent signaling pathway (25), and that APN promotes endothelial cell survival, migration, and differentiation into capillary-like structures (37, 42). We therefore sought to determine the contribution of APN to tumor-associated angiogenesis. Our experiments suggest that APN supports the release of angiogenic factors such as VEGF-A and VEGF-B and can promote blood vessel formation as judged by an increase in endothelial cell markers such as CD31 and von Willebrand factor in the PyMT mammary tumors relative to PyMT/ APN KO–derived tumors. Our experiments using Matrigel implants suggest potent effects of APN that can lead to extensive reprogramming and induction of blood vessel formation. Importantly, these experiments, together with the data obtained from our microarray analysis on WT animals injected with APN, suggest a direct role for APN in the angiogenic response by paracrine and/or endocrine effects on cell types such as endothelial cells and inflammatory cells, rather than mediating its effects exclusively through action on the cancer cells.

It is generally accepted that obesity is a risk factor for breast cancer in postmenopausal, but not premenopausal women (13). Because APN levels are inversely correlated with obesity (11), it has been suggested that the decreased levels of APN may explain the increased risk of breast cancer with obesity (14, 15). In fact, numerous retrospective case-controls studies and a recent prospective study have shown that APN is inversely associated with breast cancer risk, an association that might be stronger for postmenopausal women (14, 15). Several observations in the PyMT model are consistent with this inverse association: (*a*) a robust decline in circulating APN levels that is observed as the tumor progresses and (*b*) an acceleration of mammary tumorigenesis in PyMT/APN KO compared with PyMT in

advanced malignant stages of the disease. However, similar to the differential effect of menopausal status in women, a thorough analysis of the PyMT tumor model indicates a complex role for APN, suggesting a possibly biphasic effect of APN on tumor progression or, alternatively, the development of an adaptive mechanism at late stages to bypass the dependence of APN-driven angiogenesis. The switch from a lagging to a more aggressive tumor growth rate may be a reflection of a Darwinian dynamic similar to what is observed under conditions of exposure to angiogenesis inhibitors, during which tumors acquire the ability to survive and proliferate within the suboptimal tumor microenvironment by activating alternative ways to sustain tumor growth and angiogenesis (26, 36, 43). Similarly, our data imply that following a prolonged antiangiogenic stress due to the absence of APN, an adaptive resistant mechanism takes place. A detailed gene expression analysis of the tumors arising in the PyMT/APN KO mice at late stages reveals easily interpretable changes in critical genes involved in cancer growth, survival, and enhanced glycolysis. In line with data that VEGF-A and SDF-1 can induce recruitment of endothelial progenitor cells (4, 44, 45), we show an increase in local VEGF-A in late-stage APN KO tumor–bearing mice that potentially play a role in the observed robust mobilization of CEPs. This subpopulation of CEPs has the capacity to enhance tumor growth and has been postulated to be crucial in situations such as relapse after tumor shrinkage brought about by surgery or antiangiogenic therapies (27, 28, 38, 46). These results raise the possibility that the recruitment of this subpopulation contributes functionally to tumor growth in the PyMT/APN KO animals at late stage, rescuing the cells from their original nutrient-deprived status.

APN critically modulates insulin resistance, atherogenesis, and cardiac remodeling (11). Our data presented here indicate that it also functions as an angiogenic mediator in mammary tumors. Our work suggests that vessel development is impaired in mammary tumors lacking systemic APN, leading to a nutrient-deprived tumor at the early malignant stages. Yet, alternative pathways are activated at later stages of tumorigenesis to bypass the dependence on APN and allow for further fueling of tumor growth. Compounds that modulate its circulating levels such as the PPARγ agonists thiazolindinediones (34, 35) may have a profound effect on mammary tumorigenesis through the angiogenesis axis (34). Interestingly, PPARγ agonists have been shown to induce VEGF-A in adipocytes (47) and, importantly, may be involved in adipose tissue–associated angiogenesis (48). PPARγ is most abundantly expressed in adipocytes, yet it is also expressed in endothelial and tumor cells, macrophages, and a number of epithelial tissues including epithelia in the mammary gland (34). Thus, this class of drugs clearly induces pleiotropic affects in multiple tissues. Taken together, the effects of PPARγ agonists on the enhancement of mammary tumorigenesis, as judged by the analysis of these models, may be mediated in part by the cross talk between APN and the vasculature axis, stimulating tumor growth. In contrast, PPARγ may act as an antimitogenic factor in tumor cells and as an anti-inflammatory factor in macrophages (34). The net result of PPARγ stimulation on the transformed ductal epithelium of the mammary gland raises the distinct possibility that these agonists may enhance neovascularization of emerging tumors and should be used with caution in a diabetic population with newly diagnosed malignancies of the mammary gland. On the other hand, tumors arising in an environment with low APN (such as in an obese and/or diabetic population) may assume a more aggressive phenotype as suggested by the increased tumor growth at later stages in our APN KO mice.

Given that elevated levels of CEPs were observed in APN KO mice independent of the presence or absence of a tumor (data not shown), the proangiogenic role of APN may not only be relevant under tumor-associated conditions but may also contribute to its potent antidiabetic effects in our previously described mouse models with moderately elevated levels of APN achieved through transgenic overexpression. APN enables adipose tissue pads to massively expand during times of excess caloric intake, allowing a redistribution of

excess ectopic lipid deposits. Despite the massive hyperplasia of the fat pads in these mice overexpressing APN, the fat pads remain minimally inflamed and fully insulin sensitive and do not display the classic hallmarks of expansion under suboptimal conditions, such as hypoxia and macrophage infiltration (29).

Collectively, our detailed analysis suggests several possible strategies to delay an acquired adaptation to antiangiogenic stress under conditions when APN abundance is low, such as in the context of obesity. This includes treatment regimens targeting CEPs, an approach that has previously been shown to enhance treatment efficacy of cytotoxic chemotherapy (49). These patients may potentially also show higher sensitivity to chemotherapy given their normalized vasculature (46, 50). A molecular understanding of the APN-mediated proangiogenic activity combined with the identification of key stimulating factors that are turned on at advanced stages of the disease has the potential to reveal novel therapeutic approaches for breast cancer in blocking both the angiogenic switch and the specific adaptive pathways that are triggered as a result of chronic angiogenic stress and nutrient deprivation.

Supplementary Material

Refer to Web version on PubMed Central for supplementary material.

Acknowledgments

We thank the members of the Scherer laboratory for discussions; Michael Cammer and Yan Deng from the Analytical Imaging Facility at Albert Einstein College of Medicine, the Albert Einstein College of Medicine Diabetes Research and Training Center and Radioimmunoprecipitation Assay Core Facility (Robin Sgueglia); the University of Texas Southwestern Metabolic Core for phenotyping efforts; Dr. Quan Li from the University of Texas Southwestern Microarray Core Facility; Bei B. Zhang and John Thompson for microarray processing; the Rosetta Gene Expression Laboratory; Dr. Rani Sellers from the Histopathology Facility at Albert Einstein College of Medicine for expert help; Nils Halberg for statistical analysis; and Jiufeng Li, Aisha Cordero, and Yuan Xin for technical assistance.

Grant support: NIH grant R01-CA112023 (P.E. Scherer) and Training Program in Cellular and Molecular Biology and Genetics Grant T32-GM04791 (S. Landskroner-Eiger).

References

1. Scherer PE. Adipose tissue: from lipid storage compartment to endocrine organ. Diabetes. 2006; 55:1537–45. [PubMed: 16731815]
2. Rosen ED, Spiegelman BM. Adipocytes as regulators of energy balance and glucose homeostasis. Nature. 2006; 444:847–53. [PubMed: 17167472]
3. Trujillo ME, Scherer PE. Adipose tissue-derived factors: impact on health and disease. Endocr Rev. 2006; 27:762–78. [PubMed: 17056740]
4. Orimo A, Gupta PB, Sgroi DC, et al. Cell. 2005; 121:335–48. [PubMed: 15882617]
5. Iyengar P, Combs TP, Shah SJ, et al. Adipocyte-secreted factors synergistically promote mammary tumorigenesis through induction of anti-apoptotic transcriptional programs and proto-oncogene stabilization. Oncogene. 2003; 22:6408–23. [PubMed: 14508521]
6. Lin EY, Li JF, Gnatovskiy L, et al. Macrophages regulate the angiogenic switch in a mouse model of breast cancer. Cancer Res. 2006; 66:11238–46. [PubMed: 17114237]
7. Iyengar P, Espina V, Williams TW, et al. Adipocyte-derived collagen VI affects early mammary tumor progression *in vivo*, demonstrating a critical interaction in the tumor/stroma microenvironment. J Clin Invest. 2005; 115:1163–76. [PubMed: 15841211]
8. Scherer PE, Williams S, Fogliano M, Baldini G, Lodish HF. A novel serum protein similar to C1q, produced exclusively in adipocytes. J Biol Chem. 1995; 270:26746–9. [PubMed: 7592907]
9. Berg AH, Combs TP, Du X, Brownlee M, Scherer PE. The adipocyte-secreted protein Acrp30 enhances hepatic insulin action. Nat Med. 2001; 7:947–53. [PubMed: 11479628]

10. Combs TP, Berg AH, Obici S, Scherer PE, Rossetti L. Endogenous glucose production is inhibited by the adipose-derived protein Acrp30. J Clin Invest. 2001; 108:1875–81. [PubMed: 11748271]
11. Trujillo ME, Scherer PE. Adiponectin—journey from an adipocyte secretory protein to biomarker of the metabolic syndrome. J Intern Med. 2005; 257:167–75. [PubMed: 15656875]
12. Shibata R, Sato K, Pimentel DR, et al. Adiponectin protects against myocardial ischemia-reperfusion injury through AMPK- and COX-2-dependent mechanisms. Nat Med. 2005; 11:1096–103. [PubMed: 16155579]
13. Lorincz AM, Sukumar S. Molecular links between obesity and breast cancer. Endocr Relat Cancer. 2006; 13:279–92. [PubMed: 16728564]
14. Mantzoros C, Petridou E, Dessypris N, et al. Adiponectin and breast cancer risk. J Clin Endocrinol Metab. 2004; 89:1102–7. [PubMed: 15001594]
15. Tworoger SS, Eliassen AH, Kelesidis T, et al. Plasma adiponectin concentrations and risk of incident breast cancer. J Clin Endocrinol Metab. 2007; 92:1510–6. [PubMed: 17213279]
16. Wang Y, Lam JB, Lam KS, et al. Adiponectin modulates the glycogen synthase kinase-3β/β-catenin signaling pathway and attenuates mammary tumorigenesis of MDA-MB-231 cells in nude mice. Cancer Res. 2006; 66:11462–70. [PubMed: 17145894]
17. Dieudonne MN, Bussiere M, Dos Santos E, et al. Adiponectin mediates antiproliferative and apoptotic responses in human MCF7 breast cancer cells. Biochem Biophys Res Commun. 2006; 345:271–9. [PubMed: 16678125]
18. Brakenhielm E, Veitonmaki N, Cao R, et al. Adiponectin-induced antiangiogenesis and anti-tumor activity involve caspase-mediated endothelial cell apoptosis. Proc Natl Acad Sci U S A. 2004; 101:2476–81. [PubMed: 14983034]
19. Talmadge JE, Singh RK, Fidler IJ, Raz A. Murine models to evaluate novel and conventional therapeutic strategies for cancer. Am J Pathol. 2007; 170:793–804. [PubMed: 17322365]
20. Sikder H, Huso DL, Zhang H, et al. Disruption of Id1 reveals major differences in angiogenesis between transplanted and autochthonous tumors. Cancer Cell. 2003; 4:291–9. [PubMed: 14585356]
21. Nawrocki AR, Rajala MW, Tomas E, et al. Mice lacking adiponectin show decreased hepatic insulin sensitivity and reduced responsiveness to peroxisome proliferator–activated receptor γ agonists. J Biol Chem. 2006; 281:2654–60. [PubMed: 16326714]
22. Guy CT, Cardiff RD, Muller WJ. Induction of mammary tumors by expression of polyoma-virus middle T oncogene: a transgenic mouse model for metastatic disease. Mol Cell Biol. 1992; 12:954–61. [PubMed: 1312220]
23. Lin EY, Jones JG, Li P, et al. Progression to malignancy in the polyoma middle T onco-protein mouse breast cancer model provides a reliable model for human diseases. Am J Pathol. 2003; 163:2113–26. [PubMed: 14578209]
24. Maeda N, Shimomura I, Kishida K, et al. Diet-induced insulin resistance in mice lacking adiponectin/ACRP30. Nat Med. 2002; 8:731–7. [PubMed: 12068289]
25. Shibata R, Ouchi N, Kihara S, et al. Adiponectin stimulates angiogenesis in response to tissue ischemia through stimulation of amp-activated protein kinase signaling. J Biol Chem. 2004; 279:28670–4. [PubMed: 15123726]
26. Bergers G, Hanahan D. Modes of resistance to anti-angiogenic therapy. Nat Rev Cancer. 2008; 8:592–603. [PubMed: 18650835]
27. Bertolini F, Shaked Y, Mancuso P, Kerbel RS. The multifaceted circulating endothelial cell in cancer: towards marker and target identification. Nat Rev Cancer. 2006; 6:835–45. [PubMed: 17036040]
28. Ruzinova MB, Schoer RA, Gerald W, et al. Effect of angiogenesis inhibition by Id loss and the contribution of bone-marrow-derived endothelial cells in spontaneous murine tumors. Cancer Cell. 2003; 4:277–89. [PubMed: 14585355]
29. Kim JY, van de Wall E, Laplante M, et al. Obesity-associated improvements in metabolic profile through expansion of adipose tissue. J Clin Invest. 2007; 117:2621–37. [PubMed: 17717599]
30. Weidner N, Semple JP, Welch WR, Folkman J. Tumor angiogenesis and metastasis-correlation in invasive breast carcinoma. N Engl J Med. 1991; 324:1–8. [PubMed: 1701519]

31. Wang ZV, Schraw TD, Kim JY, et al. Secretion of the adipocyte-specific secretory protein adiponectin critically depends on thiol-mediated protein retention. Mol Cell Biol. 2007; 27:3716–31. [PubMed: 17353260]
32. Hughes TR, Mao M, Jones AR, et al. Expression profiling using microarrays fabricated by an ink-jet oligonucleotide synthesizer. Nat Biotechnol. 2001; 19:342–7. [PubMed: 11283592]
33. Rosen ED, Spiegelman BM. PPARγ: a nuclear regulator of metabolism, differentiation, and cell growth. J Biol Chem. 2001; 276:37731–4. [PubMed: 11459852]
34. Michalik L, Desvergne B, Wahli W. Peroxisome-proliferator-activated receptors and cancers: complex stories. Nat Rev Cancer. 2004; 4:61–70. [PubMed: 14708026]
35. Combs TP, Wagner JA, Berger J, et al. Induction of adipocyte complement-related protein of 30 kilodaltons by PPARγ agonists: a potential mechanism of insulin sensitization. Endocrinology. 2002; 143:998–1007. [PubMed: 11861525]
36. Gatenby RA, Gillies RJ. Why do cancers have high aerobic glycolysis? Nat Rev Cancer. 2004; 4:891–9. [PubMed: 15516961]
37. Ouchi N, Kobayashi H, Kihara S, et al. Adiponectin stimulates angiogenesis by promoting cross-talk between AMP-activated protein kinase and Akt signaling in endothelial cells. J Biol Chem. 2004; 279:1304–9. [PubMed: 14557259]
38. Lyden D, Hattori K, Dias S, et al. Impaired recruitment of bone-marrow-derived endothelial and hematopoietic precursor cells blocks tumor angiogenesis and growth. Nat Med. 2001; 7:1194–201. [PubMed: 11689883]
39. Sengenes C, Miranville A, Maumus M, et al. Chemotaxis and differentiation of human adipose tissue $CD34^{+}/CD31^{-}$ progenitor cells: role of stromal derived factor-1 released by adipose tissue capillary endothelial cells. Stem Cells. 2007; 25:2269–76. [PubMed: 17525234]
40. Du R, Lu KV, Petritsch C, et al. HIF1α induces the recruitment of bone marrow-derived vascular modulatory cells to regulate tumor angiogenesis and invasion. Cancer Cell. 2008; 13:206–20. [PubMed: 18328425]
41. Hebbard LW, Garlatti M, Young LJ, et al. T-cadherin supports angiogenesis and adiponectin association with the vasculature in a mouse mammary tumor model. Cancer Res. 2008; 68:1407–16. [PubMed: 18316604]
42. Kobayashi H, Ouchi N, Kihara S, et al. Selective suppression of endothelial cell apoptosis by the high molecular weight form of adiponectin. Circ Res. 2004; 94:e27–31. [PubMed: 14752031]
43. Gatenby RA, Gillies RJ. A microenvironmental model of carcinogenesis. Nat Rev Cancer. 2008; 8:56–61. [PubMed: 18059462]
44. Hattori K, Dias S, Heissig B, et al. Vascular endothelial growth factor and angiopoietin-1 stimulate postnatal hematopoiesis by recruitment of vasculogenic and hematopoietic stem cells. J Exp Med. 2001; 193:1005–14. [PubMed: 11342585]
45. Asahara T, Takahashi T, Masuda H, et al. VEGF contributes to postnatal neovascularization by mobilizing bone marrow-derived endothelial progenitor cells. EMBO J. 1999; 18:3964–72. [PubMed: 10406801]
46. Batchelor TT, Sorensen AG, di Tomaso E, et al. AZD2171, a pan-VEGF receptor tyrosine kinase inhibitor, normalizes tumor vasculature and alleviates edema in glioblastoma patients. Cancer Cell. 2007; 11:83–95. [PubMed: 17222792]
47. Emoto M, Anno T, Sato Y, et al. Troglitazone treatment increases plasma vascular endothelial growth factor in diabetic patients and its mRNA in 3T3-1 adipocytes. Diabetes. 2001; 50:1166–70. [PubMed: 11334422]
48. Fukumura D, Ushiyama A, Duda DG, et al. Paracrine regulation of angiogenesis and adipocyte differentiation during *in vivo* adipogenesis. Circ Res. 2003; 93:e88–97. [PubMed: 14525808]
49. Shaked Y, Henke E, Roodhart JM, et al. Rapid chemotherapy-induced acute endothelial progenitor cell mobilization: implications for anti-angiogenic drugs as chemosensitizing agents. Cancer Cell. 2008; 14:263–73. [PubMed: 18772115]
50. Stockmann C, Doedens A, Weidemann A, et al. Deletion of vascular endothelial growth factor in myeloid cells accelerates tumorigenesis. Nature. 2008; 456:814–8. [PubMed: 18997773]

Translational Relevance

The contributions of stromal adipocytes toward mammary tumor growth have been appreciated for decades. The effects of adiponectin (APN) on tumor cells are not well understood, but a number of cancer epidemiologic studies have focused on APN as a predictive marker. APN levels are becoming a popular and widely measured clinical parameter, including in the context of breast cancer studies. Here, we present the first *in vivo* data on the role of APN on mammary tumor growth and highlight its function as a potent proangiogenic factor. APN is a key mediator of the antidiabetic actions of the widely used peroxisome proliferator–activated receptor γ agonists (thiazolindinediones). These compounds lead to an increased tumor mass in the present studies. Our data suggest a possible mechanism for the increased risk and poorer prognosis seen in breast cancer patients with low serum APN levels (such as obese women) due to acquired adaptation of tumors to antiangiogenic stress.

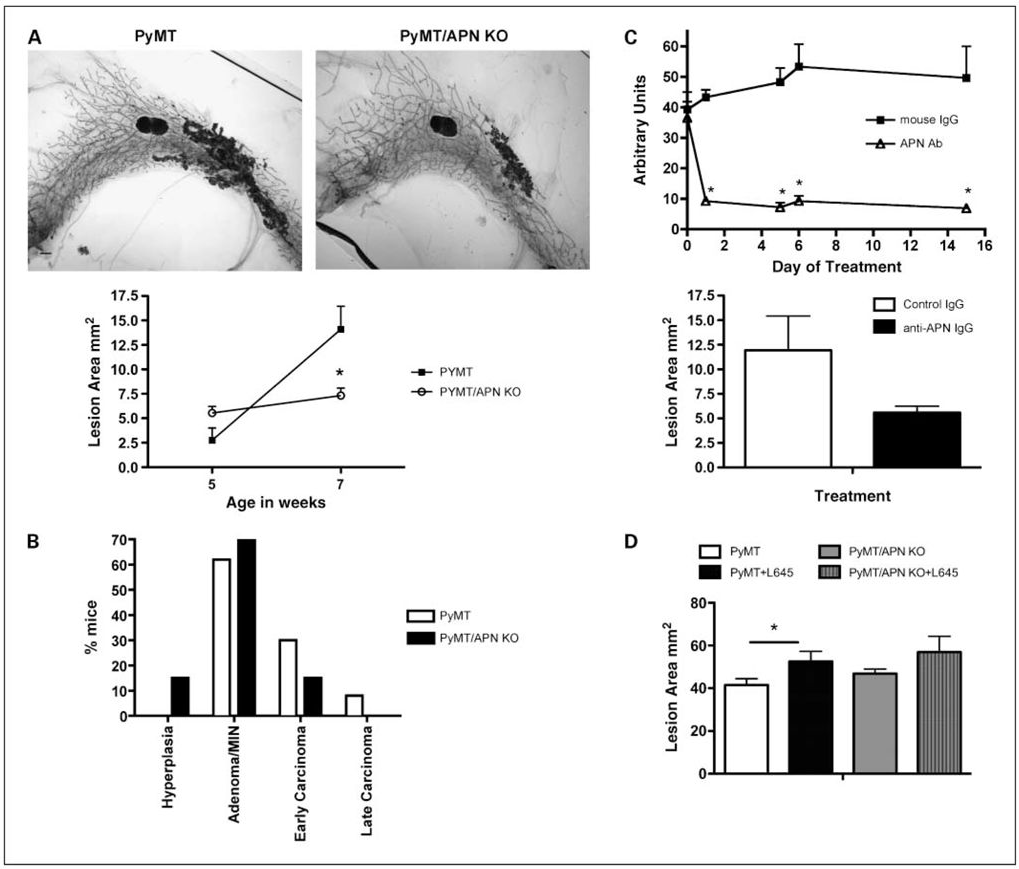

Fig. 1.

PyMT/APN KO mice display delayed mammary tumor progression. *A*, top, representative whole-mount preparations of inguinal mammary gland derived from age-matched 7-wk-old mice. Bar, 1 mm. Bottom, total lesion area of PyMT and PyMT/APN KO at 5 wk (n = 4–6 per group) and 7 wk (n = 11–12 per group; *bars*, SE; *, $P < 0.05$). *B*, summary of tumor staging distribution derived from H&E of 7-wk-old inguinal mammary glands sections (n = 13 per group). *C*, a representative experiment is shown at the top. Western blot quantification of circulating APN levels in mice treated with monoclonal antibodies neutralizing APN (*bars*, SE; *, $P < 0.001$, two-way ANOVA). Bottom, APN neutralizing antibody–treated mice (n = 6) show a trend of a 2-fold decrease in lesion area compared with IgG-treated mice (n = 3) as measured in whole mounts of inguinal mammary glands (*bars*, SE; $P = 0.2$). *D*, mice were treated with either vehicle or the PPARγ agonist COOH from 4 to 9 wk of age. Total lesion area from whole mounts was measured. PyMT mice treated with the PPARγ agonist have a 35% increase in lesion area compared with vehicle-treated PyMT, whereas PyMT/APN KO mice treated with the PPARγ agonist show a more modest increase in lesion area compared with the untreated PyMT/APN KO group (n = 9–10 per group; *bars*, SE; *, $P < 0.05$).

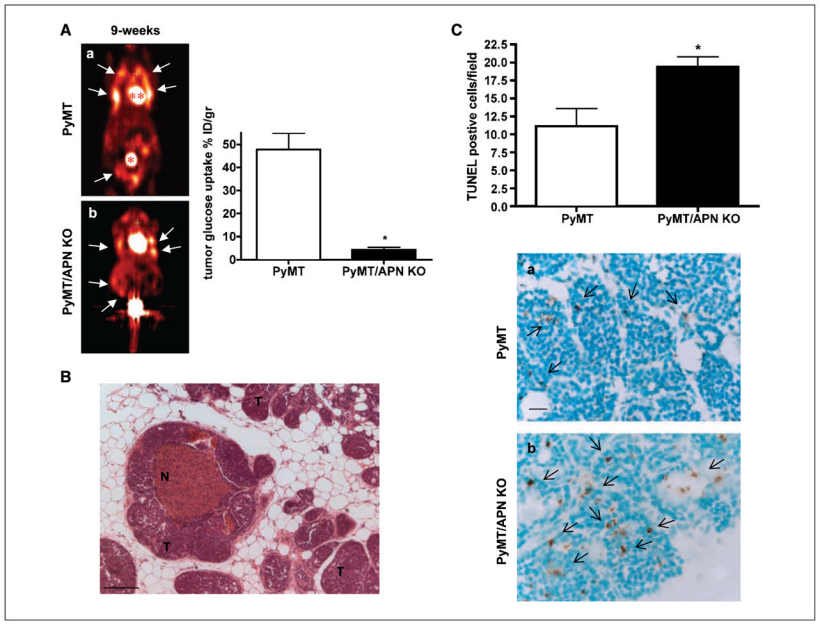

Fig. 2.

Decreased accumulation of [^{18}F]FDG as assessed by microPET and increased tumor-associated death in PyMT/APN KO tumor–bearing mice. *A*, coronal images showing the mammary tumor spread (*arrows*) in addition to bladder (*) and heart (**) that have a high glucose uptake. By 9 wk of age, PyMT mice (n = 4–5) displayed an 11-fold increase in [^{18}F]FDG uptake in the mammary glands compared with age-matched PyMT/APN KO mice (*a* and *b; n* = 4; *bars*, SE; *, $P < 0.05$). *B*, H&E staining showing necrotic regions (*N*) in mammary tumors (*T*) lacking APN; no necrotic regions were observed in age-matched mammary tumors of PyMT mice (n = 21 per group). *C*, quantitative analysis of TUNEL staining in 9-wk-old PyMT mice and PyMT/APN KO mice (n = 6 per group; *bars*, SE; *, $P < 0.05$). Bar, 100 μm (*B*), 20 μm (*C*).

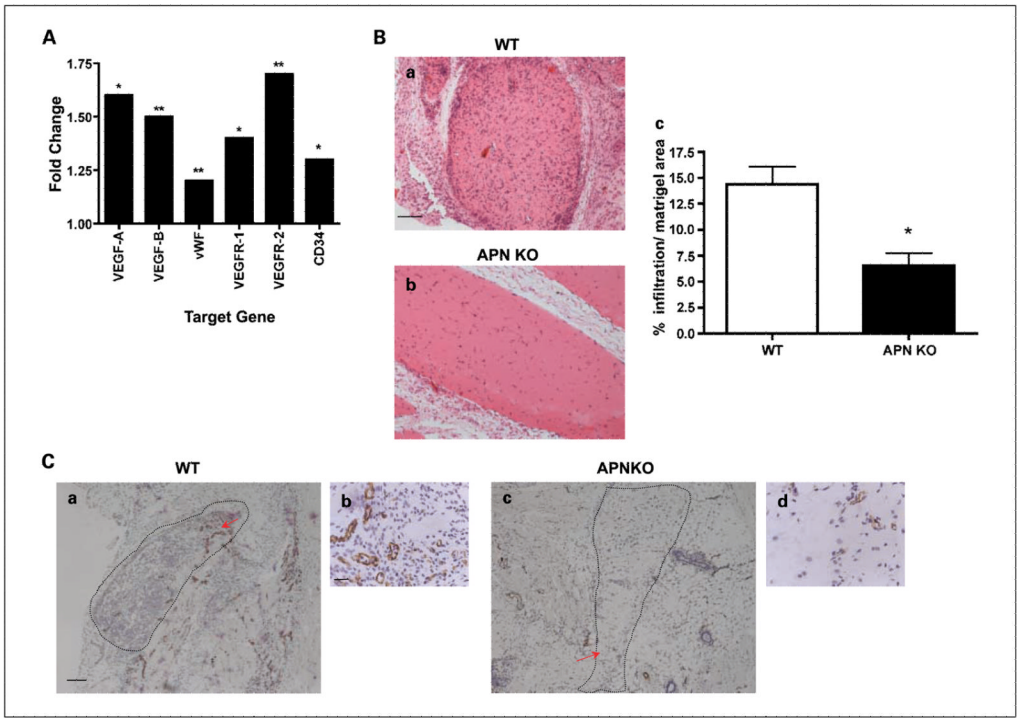

Fig. 3.

APN as a positive regulator of angiogenesis independent of tumor cells. *A*, gene expression profiling of the epididymal fat tissue was determined by microarray analysis. Results are expressed as the fold change in gene expression in WT mice treated with APN injections compared with WT mice treated with vehicle ($n = 3$ per treated group, $n = 10$ per control group). *, $P < 0.005$; **, $P < 0.01$. *B* and *C*, mice were s.c. injected with Matrigel + basic FGF. *B*, a representative H&E staining of the Matrigel matrix (*a* and *b*). Image J quantification shows a >2-fold difference between the WT and APN KO Matrigel cellular content (*c; bars*, SE; *, $P < 0.05$; $n = 6$ per group). *C*, a representative immunohistochemical staining for CD31 endothelium ($n = 4$ per group). Dashed lines, Matrigel region. Red arrow, enlarged section. Bar, 100 μm [*C* (*a* and *c*)]; 20 μm [*B* (*a* and *b*) and *C* (*b* and *d*)].

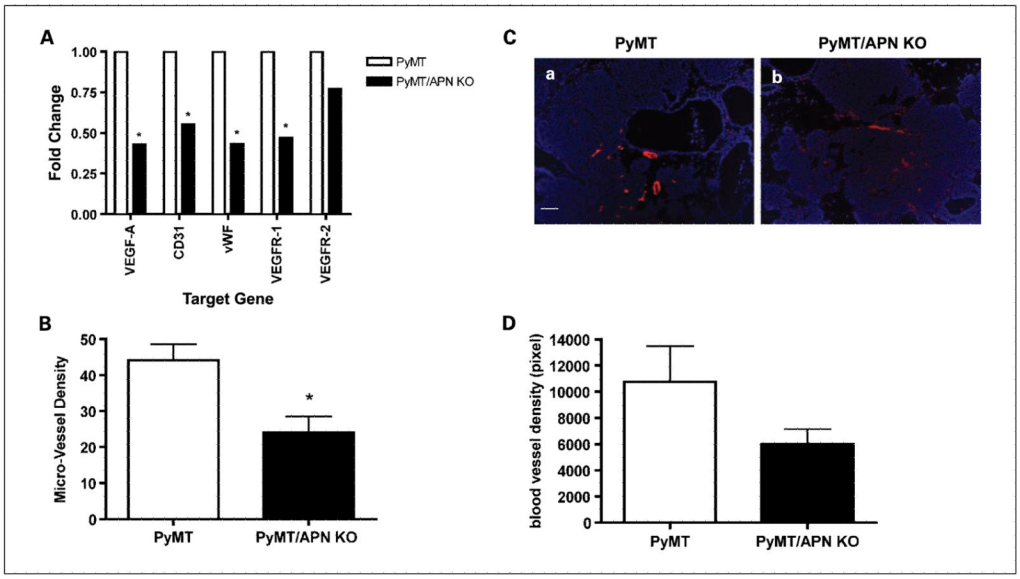

Fig. 4.

PyMT/APN KO show a decrease in the angiogenic profile. *A*, mammary glands were excised and mRNA levels were quantified by real-time PCR; β-actin was used as an internal control (*, $P < 0.05$; $n = 5–8$ per group). *B*, immunohistochemistry analysis of CD31 endothelium (*bars*, SE; *, $P < 0.05$; $n = 5$ per group). *C*, vessel density evaluation in tumor sections from Texas red-dextran–injected mice counterstained with 4′,6-diamidino-2-phenylindole. Bar, 50 μm. *D*, inguinal mammary gland was imaged for vessel density distribution and compared between PyMT ($n = 7$) and PyMT/APN KO mice ($n = 5$; *bars*, SE; $P = 0.15$).

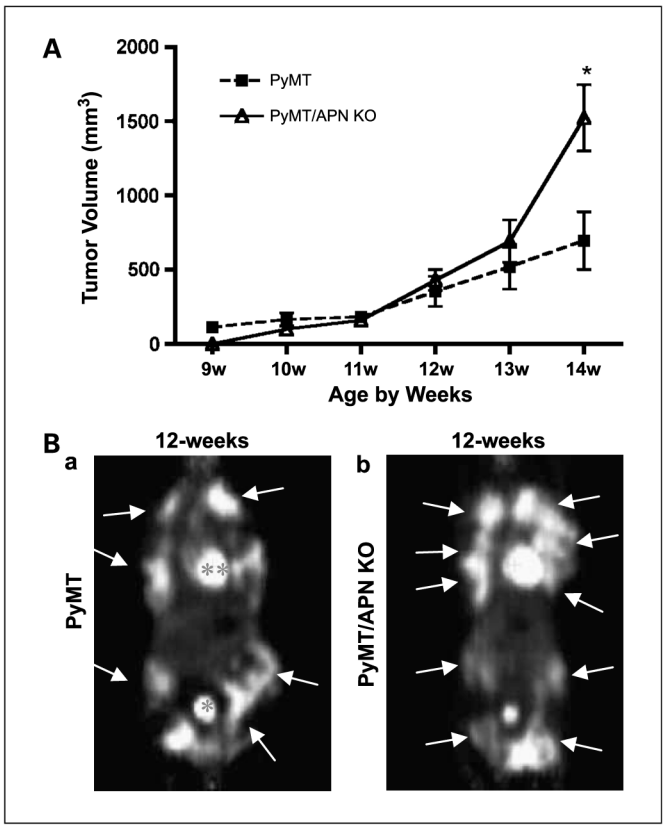

Fig. 5.

Late-stage tumorigenesis: PyMT/APN KO mice display an adaptive phenotype. *A*, average values are presented for the longitudinal measurements of the first palpable tumors. PyMT, $n = 28$; PyMT/APN KO, $n = 21$ (*bars*, SE; *, $P < 0.05$, two-way ANOVA). *B*, coronal images showing the mammary tumor spread (*arrows*) in addition to bladder (*) and heart (**) that have a high glucose uptake as measured by microPET. Twelve-week-old PyMT/APN KO mice ($n = 4$) showed comparable glucose uptake to PyMT mice ($n = 7$).

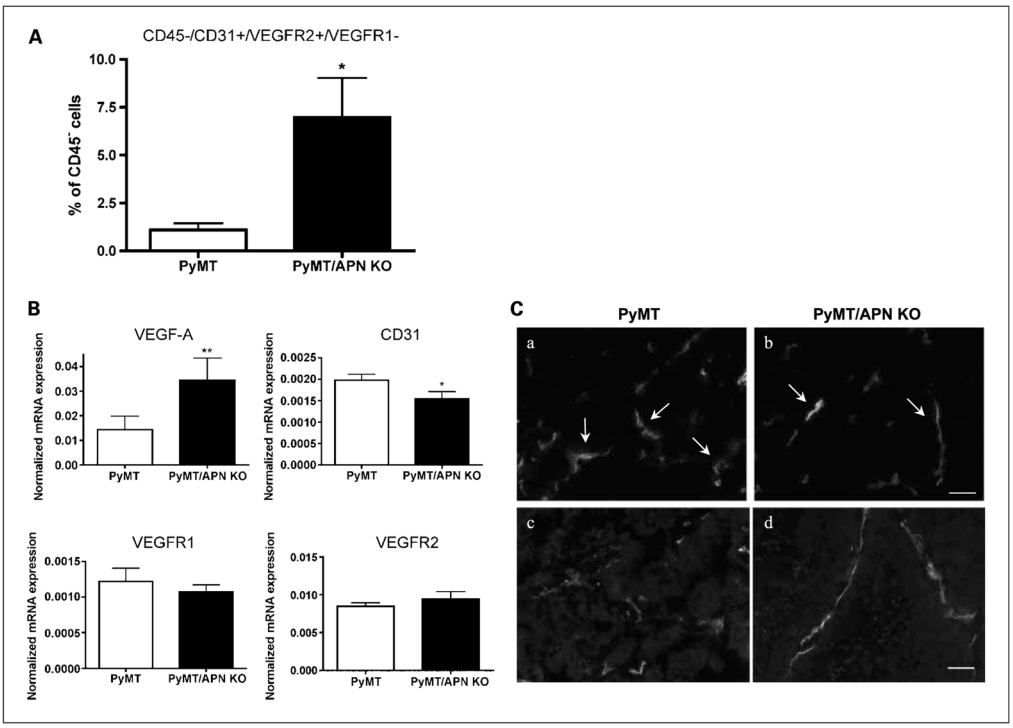

Fig. 6.

PyMT/APN KO mice initiate mobilization of circulating endothelial progenitor cells during late-stage tumorigenesis. *A*, fluorescence-activated cell sorting analysis of CEPs levels in circulation, showing a 6-fold increase in PyMT/APN KO compared with PyMT mice (*bars*, SE; *, $P < 0.05$; $n = 5–7$ mice per group). *B*, inguinal mammary tumors were excised and mRNA levels were quantified by real-time PCR (**, $P = 0.07$; *, $P < 0.05$; $n = 5–7$ per group). *C*, tumors were imaged for blood vessel morphology using CD31 antibody. PyMT tumors exhibited dilated and torturous tumor vessels (*a*, *c*). In contrast, PyMT/APN KO blood vessels showed slim and elongated characteristics (*b*, *d; n* = 4 per group). Bar, 50 μm.

Table 1

Differential gene expression in PyMT/APN KO versus PyMT in late-stage tumors

Cluster	Gene name	Accession no.	Fold change
Genes up-regulated in PyMT/APN KO tumors			
Cancer	*ST6GAL1*	NM_1459332.2	1.6
	HIF1a	NM_010431.1	1.5
	MAPKS1P1	NM_011162.2	1.5
	PGK1	NM_008828.2	1.5
	PTGS1	NM_008969.1	1.3
	CXCR4	NM_009911.2	1.3
	HDAC5	NM_010412.2	1.3
	CDKN1B	NM_009875.2	1.2
Cell death	*BFAR*	NM_025976	4.5
	DD1T4	NM_029083.1	1.6
	LGALS7	NM_008496.4	1.6
	MAPK81P1	NM_011162.2	1.5
	MMP13	NM_008607.1	1.3
Glycolysis	*PGK1*	NM_008828.2	1.5
	TP11	NM_009415.1	1.4
Genes down-regulated in PyMT/APN KO tumors			
Cancer	*FGF1*	NM_010197.2	2.9
	MMP2	NM_008610.1	1.6
	AXL	A1323647	1.5
	CAV1	NM_007616.2	1.4
	RB1	NM_009029.1	1.3
	CCR5	NM_9919.2	1.3
	MMP1	NM_032006.2	1.2
	TLR4	NM_021297.1	1.2
Cell death	*TNFRSF10*	NM_020275.3	1.6
	IL15RA	NM_133836.1	1.4